Young, J. D., Staniforth, M., Dean, J. C., Roberts, G. M., Mazzoni, F., Karsili, T. N. V., Ashfold, M. N. R., Zwier, T. S., & Stavros, V. G. (2014). Towards Understanding Photodegradation Pathways in Lignins: The Role of Intramolecular Hydrogen Bonding in Excited States. *Journal of Physical Chemistry Letters*, *5*(12), 2138-2143. https://doi.org/10.1021/jz500895w

Towards understanding photodegradation pathways in lignins: The role of intramolecular hydrogen-bonding in excited states

Jamie D. Young[†], Michael Staniforth[†], Jacob C. Dean[§], Gareth M. Roberts[†], Federico Mazzoni[‡], Tolga N.V. Karsili,[#] Michael N.R. Ashfold,[#] Timothy S. Zwier[§], and Vasilios G. Stavros[†]*

[†]Department of Chemistry, University of Warwick, Library Road, Coventry, CV4 7AL, UK.

[‡]Lens, Polo Scientifico e Tecnologico dell'Universitá di Firenze, Via Nello Carrara 1, 50019 Sesto Fiorentino (FI), Italy and Dipartimento di Chemica, Polo Scientifico e Tecnologico dell'Universitá di Firenze, Via della Lastruccia 3, 50019 Sesto Fiorentino (FI), Italy.

[§]Department of Chemistry, Purdue University, West Lafayette, Indiana 47907-2084, United States.

[#] School of Chemistry, University of Bristol, Cantock's Close, Bristol, BS8 1TS, U.K.

ABSTRACT: The photoinduced dynamics of the lignin building blocks syringol, guaiacol and phenol were studied using time-resolved ion yield spectroscopy and time-resolved velocity map imaging. Following irradiation of syringol and guaiacol with ultraviolet light, the excited state dynamics display a quantum beat pattern attributed to OH and OMe torsion and OMe flapping motions. We attribute this behavior to changes in the geometry of the S_0, S_1 and D_0 of syringol and guaiacol. In syringol, H-atom elimination is observed at excitation wavelengths encapsulating these modes, having a direct effect on the photostability of the molecule. From these results we develop a more intimate structure-dynamics-function understanding of photodegradation in lignins.

Second only to cellulose, lignin is the most abundant naturally occurring biopolymer on Earth.[1] Present in the cell walls of all vascular plants, it is responsible for providing structural support, water transport and protection against microorganisms.[1-5] However, due to the heterogeneous nature of the polymer itself, our knowledge of the precise macromolecular structure of lignin is still lacking. It is known that across different plant species, the various structures, and properties associated with them, are dictated by the stoichiometric proportions of just three monomers: *p*-coumaryl, coniferyl and sinapyl alcohols, termed monolignols.[5,6]

Despite the importance of these molecules, very little is known about the photochemistry of lignin, or the monolignols themselves. Previous high-resolution spectroscopy measurements have been carried out on the closely related analogues *p*-vinylphenol,[7,8] *p*-coumaric acid,[9] and *o*-methoxyphenol (guaiacol).[10] More recently, Zwier and co-workers have reported the first spectroscopic study of the monolignols and β-O-4/β-β dilignols.[11,12] These studies have provided new insights to the conformer-specific spectroscopies of model lignins, potentially yielding knowledge of *structure-function* relationships in the larger polymer network through this 'bottom-up' study of the building-blocks themselves.

Here, we use an analogous reductionist approach as a stepping-stone for understanding ultraviolet (UV) induced photodegradation pathways within lignin in greater detail. Currently, it is known that one of the primary mechanisms driving this process involves the photo-catalyzed formation of phenoxyl (PhO) radical sites, generated following the loss of H-atoms, eventually leading to undesired discoloration and structural weakening.[13] With this in mind, we elect to compare and contrast the UV-induced excited state dynamics of phenol, guaiacol and syringol (Figure 1a-c), which are model chromophores of lignin, derived from *p*-coumaryl, coniferyl and sinapyl alcohols, respectively. Unlike phenol, the presence of the methoxy-group(s) in guaiacol and syringol, *ortho* to the hydroxy-group, leads to an intramolecular H-bond between these two functional moieties, which distorts the geometry from planarity in the first electronically excited ππ* state (S_1), relative to the planar ground state (S_0) structure (Figure 1d-f).[11,14] In this contribution, we demonstrate how the different molecular structures of these three UV chromophores in their S_1 states – specifically, the degree of H-bonding – can dramatically influence their excited state dynamics, and in turn the relative propensities for forming PhO sites (*i.e.* their relative 'photostabilities'), thereby taking a first step towards a more com-

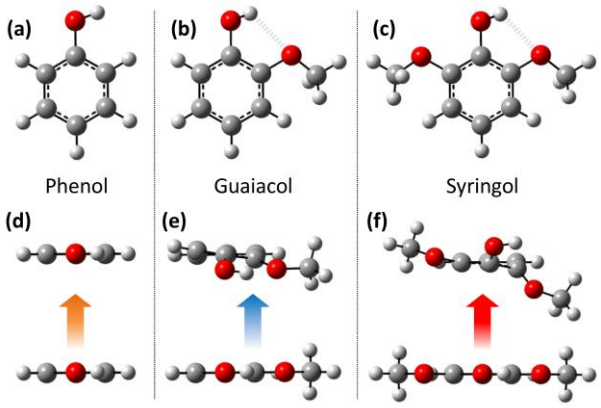

Figure 1. (a-c) Chemical structures of the three monolignol chromophores (d-f) and their molecular geometries in both the ground and excited states of the neutral molecule, S_0 and S_1 respectively.

plete structure-*dynamics*-function picture of photodegradation in lignin.

The detailed experimental procedure has been described elsewhere[15,16] and in the SI. The techniques implemented are time-resolved ion-yield (TR-IY) spectroscopy[17] and velocity map ion imaging (VMI).[18] Following excitation of phenol, guaiacol or syringol using a broadband (~500 cm^{-1}) femtosecond (fs) pulses, a coherent superposition of low frequency Franck-Condon (FC) active modes are excited in the S_1 state, preparing a vibrational wavepacket.[19] As this wavepacket evolves over time, it is then projected (photoionized) onto the ground state of the cation (D_0) using a second time-delayed (Δt) fs probe pulse, and the resulting parent$^+$ ion signal is recorded as a function of Δt. The pump and probe pulses intercept a molecular beam of target molecules seeded in helium. The pump pulse is centered around the S_1 origin band whilst the probe pulse is tuned to photoionize slightly above the adiabatic ionization potential (IP_{ad}) of the molecule of interest. VMI is also used to monitor any loss of H-atoms after excitation. Any H-atoms are resonantly ionized to form H^+ with a 243 nm probe pulse at Δt = 1.2 ns. H^+ is then detected using VMI, and the recorded 2-D H^+ velocity map images transformed into desired 1-D total kinetic energy release (TKER) spectra using an image reconstruction algorithm[20] and Jacobian.

We begin our discussion with phenol, which serves as a benchmark for comparison with guaiacol and syringol. Figure 2a presents a phenol$^+$ transient (triangles and black line) following excitation at 275 nm and probing with 300 nm. The IP_{ad} of phenol is evaluated as 8.51 eV[21] and thus the combined photon energy of 8.64 eV (275 nm + 300 nm) means we are only slightly above the IP_{ad} by 0.13 eV. The phenol$^+$ transient is similar to those reported previously using higher probe energies,[22,23] and shows a sharp rise at Δt = 0 which then plateaus across our 5 ps time window. This plateau is unsurprising, given that the S_1 lifetime of phenol has been previously determined as ~2.4 ns.[23] Further inspection of the transient also shows that, within the signal-to-noise, the ion signal exhibits no obvious 'quantum beating'[19] which one might anticipate if there were any large amplitude molecular rearrangements in the S_1 state (*cf.* Ref. 24). This is re-enforced by the fast Fourier transform (FFT) of this transient (Figure 2a, inset), which shows no emerging frequencies, and is also in-line with the fact that the S_0 and S_1 state geometries of phenol are similar.[25]

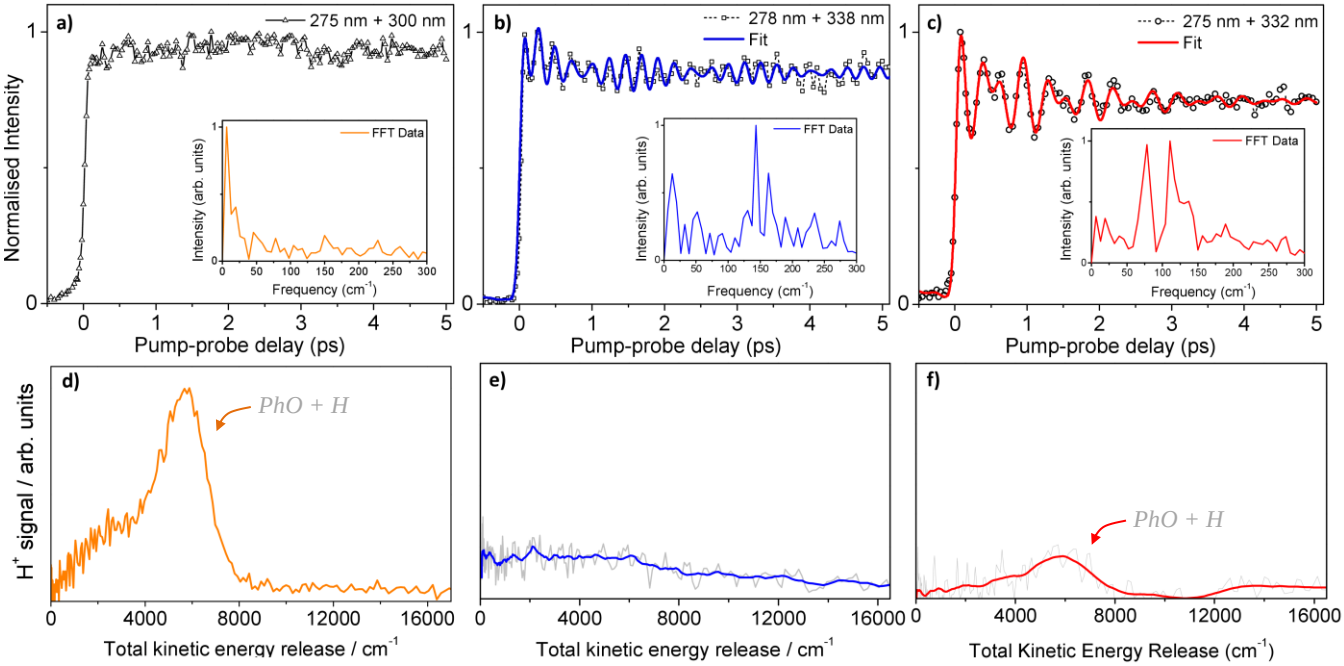

Figure 2. (a-c) Time-resolved ion yield transients collected from (a) phenol (triangles), (b) guaiacol (squares) and (c) syringol (circles) following UV excitation and subsequent probing (ionization) of the resulting parent$^+$ cation. Superimposed on the guaiacol and syringol data is the sinusoidal fit for each molecule (blue and red lines, respectively). See text for details. Inset: The FFT of the relevant transient. **(d-f)** Total kinetic energy release spectra obtained for phenol, guaiacol and syringol respectively.

Figure 2b presents a guaiacol$^+$ transient following excitation to S_1 with 278 nm and probing with 338 nm (squares and dashed line). The IP_{ad} of guaiacol is located at 7.94 eV,[26] with the combined energy of the pump and probe being 8.12 eV, yielding an excess energy of 0.18 eV. The measured transient of guaiacol$^+$ is similar to that recorded for phenol$^+$ in so much that there is an initial sharp rise at Δt = 0 which then plateaus within our 5 ps temporal window. However, the similarities with phenol cease here. Following the initial rise, the guaiacol$^+$ signal shows a small, but evident sub-1 ps decay, with a pronounced quantum beat superimposed on top. We recall that, unlike phenol, the S_1 geometry in guaiacol is non-planar (Figure 1e) in that it distorts out-of-plane in a double minimum potential well. The observed decay is thus attributed to an *overall* variation in the ionization cross-section that follows the initial geometry rearrangement out of the FC region of the initially prepared S_1 state towards the non-planar minimum (*cf.* catechol[27]).

We now consider the origins of the observed quantum beat. An analysis of the guaiacol$^+$ transient with a FFT (Figure 2b,

inset) reveals that the beat contains two dominant frequencies with associated energies of 143 cm^{-1} and 163 cm^{-1}, which correspond to wavenumber separations of vibrational eigenstates within the initially prepared wavepacket on S_1.[19] These

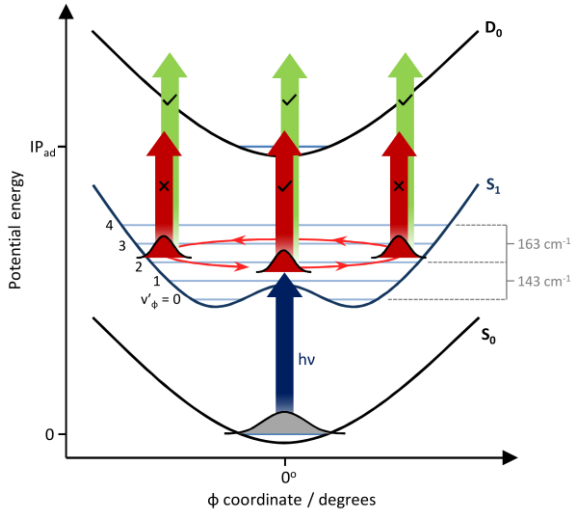

Figure 3. Schematic demonstrating the evolution of the initially excited wavepacket (red) out of the FC detection window along the φ coordinate on the S_1 potential of guaiacol.

difference frequencies align very well with the known band separations in an even quanta vibrational progression of the out-of-plane OMe 'flapping' mode (φ), which exhibits by far the largest FC activity in the REMPI/LIF spectra,[14,28,29] and highlights the *dominant* motions involved in the initial geometry rearrangement on guaiacol's S_1 surface. Combined with the strong FC activity, the pronounced beating in φ in Figure 2b can be understood with reference to the schematic in Figure 3. After excitation from the planar S_0 ground state, a vibrational wavepacket in the φ coordinate is prepared on S_1 as the geometry relaxes towards its non-planar minimum. However, the final D_0 state of guaiacol$^+$ is planar, (see SI) and the nuclear configuration is once again different, now between S_1 (non-planar) and D_0 (planar), resulting in a variable ionization cross-section to D_0 along φ as the wavepacket oscillates on S_1 (Figure 3, red arrows). Provided the vibrational wavepacket is localized (*i.e.* not dephased), this results in the characteristic beat seen in Figure 2b. Interestingly, by selecting a probe wavelength such that the combined pump and probe energy far exceeds the IP_{ad}, we find that the beats in the TR-IY signal for guaiacol$^+$ (as well as syringol$^+$ – *vide infra* and SI) vanish (*cf.* Ref 25), demonstrating the sensitivity of the detection window to the probe wavelength (Figure 3, green arrows).

We note that the broadness of the peaks in the FFT reflects the limited time window that these beats persist before they dampen out, most likely due to the rapid dephasing of the vibrational wavepacket. This proposition is reinforced by taking note of the fact that our pump is very likely exciting multiple quanta in the out-of-plane OMe 'flapping' mode (φ). Indeed, we have extended the guaiacol$^+$ transient out to 100 ps and find no evidence of revivals, suggesting that population in S_1 is channeled irreversibly into orthogonal vibrational modes. This contrasts revivals (and fractional revivals) that have been observed in electronic[30-33] and vibrational wavepackets[34-38] excited in atoms and diatomic molecules, respectively. In order to extract a time constant for the dephasing time, τ_d, we fit our measured transient to two cosine functions (with frequencies corresponding to the wavenumber separation of the vibrational states extracted from our FFT), superimposed with an exponential decay (fit details in SI). The results of this fit (Figure 2b, blue line) return a dephasing lifetime of τ_d = 3.0 ps, and we discuss the significance of this value below, in relation to the results obtained for syringol.

Figure 2c shows the syringol$^+$ transient obtained following excitation at 275 nm and probing at 332 nm (circles and dashed line). The combined photon energy of 8.2 eV is enough to surmount the ~7.9 eV IP_{ad} in syringol) (adiabatic ionization potential scan shown in SI). As with the transient observed in guaiacol (Figure 2b), following an initial sharp rise at Δt = 0, there is a clear beating in the syringol$^+$ signal that dampens by 5 ps, with no evidence of revivals (see SI). Shown inset is the FFT of the same data set, which contains two major frequency components of 78 cm^{-1} and 112 cm^{-1}. As with guaiacol, these correspond to wavenumber separations of vibrational states within the wavepacket on S_1, however, spectral congestion in the known REMPI spectrum of syringol makes assigning these modes more cumbersome.[14] Nonetheless, based on (i) the dominant FC activity of the OMe torsion (τ_{OMe}) and φ modes upon excitation to S_1[14] and (ii) the predicted geometry changes in the S_1 state of syringol (Figure 1f), these frequencies most likely arise from combination modes involving τ_{OMe} and φ, and are present in the transient for the same reasons outlined above (*cf.* Figure 3).

Once again, we fit the syringol$^+$ transient using the method described above (Figure 2c, red line) and extract a dephasing time of τ_d = 1.5 ps, noticeably faster than that observed in guaiacol (*cf.* 5.0 ps). Given that the measured REMPI spectrum of syringol is significantly more congested than that for guaiacol,[14] it is not surprising that the dephasing time determined for syringol is faster; the greater density of states in the initial superposition drives faster dephasing of the vibrational wavepacket.

Intriguingly, we see that the beats in the syringol$^+$ transient (Figure 2c), relative to the total ion signal, have greater amplitude than those observed in the guaiacol$^+$ transient (Figure 2b). We offer two possible explanations for this and discuss the validity of each in turn. The first is that in syringol, the initial composition of the wavepacket may only include a limited set of vibrational levels, composed primarily of τ_{OMe} and φ modes. However, REMPI spectra indicate that the density of vibrational states in S_1 for syringol is far greater than that of guaiacol[14], likely ruling out this conjecture. The second is that the enhanced ionization (detection) window is more localized in nuclear configuration space for syringol than in guaiacol. Credence to this argument comes from the much greater deviation from planarity in S_1 for syringol *vs* guaiacol. Indeed, time-dependent density functional theory (TD-DFT) calculations on syringol predict that following excitation from $S_1 \leftarrow S_0$, the H-bonded OMe group distorts ~50° out-of-plane in one direction, while the OH group, accompanied to a lesser extent by the 'free' OMe group, bends ~25° in the other direction (Figure 1f). The geometry change is far less pronounced for the OH and OMe groups in guaiacol. Given this fact, coupled with the planar syringol$^+$ geometry (calculated TDDFT//M05-2X/6-311++G(d,p)), the magnitude of the modulation in ionization efficiency is expected to be enhanced by virtue of the larger

displacement between S_1 and D_0 geometries in syringol. The gradual rise in ion yield, shown in the ionization efficiency scan of syringol (relative to guaiacol) near the adiabatic threshold (SI), infers such a scenario.

Given our above evidence for pronounced out-of-plane geometry changes in guaiacol and syringol's S_1 states, which is absent in phenol's, we now pose the question, how does this affect the relative propensities for photo-induced H-atom loss and formation of PhO sites in these three lignin chromophores? For phenol, recent studies demonstrate that a $^1\pi\sigma^*$ (S_2) state, which is dissociative along the O–H coordinate (see potential energy cuts in Ref. 16), is responsible for producing PhO + H species at all excitation energies above (and including) the S_1 origin (*via* either tunneling below an S_1/S_2 conical intersection at >248 nm or by ultrafast coupling onto S_2 at shorter wavelengths), as identified through the characteristic production of high kinetic energy (KE) H-atoms.[17] This is illustrated by the peak at ~7000 cm^{-1} in the representative TKER spectrum in Figure 2d. However, as the analogous TKER spectrum in Figure 2e shows, no similar high KE signature is observed for the production of PhO + H species in guaiacol. We interpret this observation to be a consequence of the intramolecular H-bond between the OH and OMe groups, which induces a barrier to O–H dissociation and aborts any formation of PhO + H products.[40] This also suggests that, despite the photo-induced geometry change inferred from our TR-IY measurements, the intramolecular H-bond between the OH and OMe groups is still maintained in the initially excited S_1 state of guaiacol. Intramolecular H-bonding is also present in the planar S_0 ground state of syringol, although our above analysis suggests that out-of-plane distortion of its OH and OMe groups in S_1 is far more dramatic than guaiacol. The TD-DFT geometry optimizations, presented in Figure 1f, demonstrate a large decrease in the proximity of the H-bonded OH and OMe moieties following photoexcitation (2.72 Å separation between the H-atom in OH and the O-atom in OMe in S_1 compared to 2.08 is S_0 with the dihedral angle between the two increasing to 70°). This will necessarily weaken the intramolecular H-bond, providing a greater potential for the now 'free' O–H bond to undergo dissociation. Indeed, the small high KE feature (~6000 cm^{-1}) present in the TKER spectrum in Figure 2f provides evidence that PhO + H photoproducts are formed from syringol, albeit with a far smaller yield than observed for phenol (*cf.* Figure 2d), which exhibits no steric/structural constraints to photo-induced O–H fission.

Given the above, we close by returning to our original question of the relative photostabilities of these three lignin chromophores. Based on the knowledge that PhO radical formation drives photodegration of the larger biopolymer, the relative photostabilities of the chromophore sites can be broadly ordered as guaiacol>syringol>phenol (in order of decreasing stability), which, with the exception of phenol, we understand to largely be dictated by the degree of H-bonding preserved after out-of-plane rearrangement in their S_1 excited states. Naturally, the findings from the present study only consider the photostability of lignin's isolated chromophores in the gas phase and select wavelengths,[40] although we note that solvation effects (*e.g.* from H_2O) are likely to be minimal given the highly hydrophobic nature of the larger biopolymer[13] suggesting the gas phase can act as a good benchmark here. More importantly though, we acknowledge that future studies of the lignin building-blocks will be important to further verify how this behavior maps onto larger components of lignin – high-resolution spectroscopy measurements already suggest that in *para* substituted analogues of these chromophores, distorted excited state geometries will still likely play a role in the ensuing dynamics.[14] With this in mind, the work here offers another key step towards developing a more intimate structure-dynamics-function understanding of photodegradation in lignin.

ASSOCIATED CONTENT

AUTHOR INFORMATION

ACKNOWLEDGMENT

J.D.Y. thanks the University of Warwick for a doctoral training award. M.S. and G.M.R thank the Leverhulme Trust and EPSRC for postdoctoral funding, respectively. V.G.S. thanks the EPSRC for an equipment grant (EP/J007153) and the Royal Society for a University Research Fellowship. J.C.D and T.S.Z thank the Department of Energy Basic Energy Sciences, Division of Chemical Sciences under Grant No. DEFG02-96ER14656.

REFERENCES

(1) Boerjan, W.; Ralph, J.; Baucher, M. *Annual Review of Plant Biology* **2003**, *54*, 519.
(2) Vanholme, R.; Demedts, B.; Morreel, K.; Ralph, J.; Boerjan, W. *Plant Physiology* **2010**, *153*, 895.
(3) Morreel, K.; Kim, H.; Lu, F.; Dima, O.; Akiyama, T.; Vanholme, R.; Niculaes, C.; Goeminne, G.; Inze, D.; Messens, E.; Ralph, J.; Boerjan, W. *Anal. Chem.* **2010**, *82*, 8095.
(4) Hage, E. R. E. v. d.; Boon, J. J.; Steenvoorden, R. J. J. M.; Weeding, T. L. *Anal. Chem.* **1994**, *66*, 543.
(5) Evtuguin, D. V.; Amado, F. M. L. *Macromolecular Bioscience* **2003**, *3*, 339.
(6) Reale, S.; Tullio, A. D.; Spreti, N.; Angelis, F. D. *Mass Spectrom. Rev.* **2004**, *23*, 87.
(7) de Groot, M.; Buma, W. J.; Gromov, E. V.; Burghardt, I.; Köppel, H.; Cederbaum, L. S. *J. Chem. Phys.* **2006**, *125*, 204303.
(8) Morgan, P. J.; Mitchell, D. M.; Pratt, D. W. *Chem. Phys.* **2008**, *347*, 340.
(9) Smolarek, S.; Vdovin, A.; Perrier, D. L.; Smit, J. P.; Drabbels, M.; Buma, W. J. *J. Am. Chem. Soc.* **2010**, *132*, 6315.
(10) Fujimaki, E.; Fujii, A.; Ebata, T.; Mikami, N. *J. Chem. Phys.* **1999**, *110*, 4238.
(11) Rodrigo, C. P.; James, W. H.; Zwier, T. S. *J. Am. Chem. Soc.* **2011**, *133*, 2632.
(12) Dean, J. C.; Walsh, P. S.; Biswas, B.; Ramachandran, P. V.; Zwier, T. S. *Chem. Sci.* **2014**. DOI: 10.1039/c3sc53260g.
(13) George, B.; Suttie, E.; Merlin, A.; Deglise, X. *Polym. Degrad. Stab.* **2005**, *88*, 268.
(14) Dean, J. C.; Navotnaya, P.; Parobek, A. P.; Clayton, R. M.; Zwier, T. S. *J. Chem. Phys.* **2013**, *139*.
(15) Iqbal, A.; Cheung, M. S. Y.; Nix, M. G. D.; Stavros, V. G. *J. Phys. Chem. A* **2009**, *113*, 8157.
(16) Wells, K. L.; Perriam, G.; Stavros, V. G. *J. Chem. Phys.* **2009**, *130*, 074308.
(17) Roberts, G. M.; Stavros, V. G. *Chem. Sci.* **2014**. DOI: 10.1039/c3sc53175a
(18) Eppink, A. T. J. B.; Parker, D. H. *Rev. Sci. Instrum.* **1997**, *68*, 3477.
(19) Zewail, A. H. *J. Phys. Chem. A* **2000**, *104*, 5660.
(20) Roberts, G. M.; Nixon, J. L.; Lecointre, J.; Wrede, E.; Verlet, J. R. R. *Rev. Sci. Instrum.* **2009**, *80*, 7.
(21) Lipert, R. J.; Colson, S. D. *J. Chem. Phys.* **1990**, *92*, 3240.

(22) Roberts, G. M.; Chatterley, A. S.; Young, J. D.; Stavros, V. G. *J. Phys. Chem. Lett.* **2012**, *3*, 348.
(23) Pino, G. A.; Oldani, A. N.; Marceca, E.; Fujii, M.; Ishiuchi, S. I.; Miyazaki, M.; Broquier, M.; Dedonder, C.; Jouvet, C. *J. Chem. Phys.* **2010**, *133*, 124313.
(24) Szarka, A. Z.; Pugliano, N.; Palit, D. K.; Hochstrasser, R. M. *Chem. Phys. Lett.* **1995**, *240*, 25.
(25) Ratzer, C.; Kupper, J.; Spangenberg, D.; Schmitt, M. *Chem. Phys.* **2002**, *283*, 153.
(26) Yuan, L.; Li, C.; Lin, J. L.; Yang, S. C.; Tzeng, W. B. *Chem. Phys.* **2006**, *323*, 429.
(27) Chatterley, A. S.; Young, J. D.; Townsend, D.; Zurek, J. M.; Paterson, M. J.; Roberts, G. M.; Stavros, V. G. *Phys. Chem. Chem. Phys.* **2013**, *15*, 6879.
(28) Wu, R. H.; Brutschy, B. *Chem. Phys. Lett.* **2004**, *390*, 272.
(29) Longarte, A.; Redondo, C.; Fernandez, J. A.; Castano, F. *J. Chem. Phys.* **2005**, *122*, *164304*.
(30) Verlet, J. R. R.; Stavros, V. G.; Minns, R. S.; Fielding, H. H. *Journal of Physics B-Atomic Molecular and Optical Physics* **2003**, *36*, 3683.
(31) Verlet, J. R. R.; Stavros, V. G.; Minns, R. S.; Fielding, H. H. *Phys. Rev. Lett.* **2002**, *89*, *263004*.
(32) Stavros, V. G.; Ramswell, J. A.; Smith, R. A. L.; Verlet, J. R. R.; Lei, J.; Fielding, H. H. *Phys. Rev. Lett.* **1999**, *83*, 2552.
(33) Wals, J.; Fielding, H. H.; Christian, J. F.; Snoek, L. C.; Vanderzande, W. J.; Vandenheuvell, H. B. V. *Phys. Rev. Lett.* **1994**, *72*, 3783.
(34) Dantus, M.; Bowman, R. M.; Zewail, A. H. *Nature* **1990**, *343*, 737.
(35) Farmanara, P.; Ritze, H. H.; Stert, V.; Radloff, W. *Chem. Phys. Lett.* **1999**, *307*, 1.
(36) Fischer, I.; Vrakking, M. J. J.; Villeneuve, D. M.; Stolow, A. *Chem. Phys.* **1996**, *207*, 331.
(37) Vrakking, M. J. J.; Villeneuve, D. M.; Stolow, A. *Phys. Rev. A* **1996**, *54*, R37.
(38) Goto, H.; Katsuki, H.; Ibrahim, H.; Chiba, H.; Ohmori, K. *Nature Physics* **2011**, *7*, 383.
(39) Yang, Y. L.; Ho, Y.-C.; Dyakov, Y. A.; Hsu, W.-H.; Ni, C.-K.; Sun, Y.-L.; Tsai, W.-C.; Hu, W.-P. *Phys. Chem. Chem. Phys.* **2013**, *15*, 7182.
(40) The present studies have focused on photoexcitation around the S_1 origin of these chromophores. At higher excitation energies we anticipate other H-atom loss channels to be active.